Statistics of cross sections of Voronoi tessellations

M. Ferraro*
Dipartimento di Fisica Sperimentale and CNISM, via P. Giuria 1, I-10125 Turin, Italy

L. Zaninetti†
Dipartimento di Fisica Generale, via P. Giuria 1, I-10125 Turin, Italy

(Received 12 May 2011; revised manuscript received 5 September 2011; published 7 October 2011)

In this paper, we investigate relationships between the volumes of cells of three-dimensional Voronoi tessellations and the lengths and areas of sections obtained by intersecting the tessellation with a randomly oriented plane. Here, in order to obtain analytical results, Voronoi cells are approximated to spheres. First, the probability density function for the lengths of the radii of the sections is derived and it is shown that it is related to the Meijer G function; its properties are discussed and comparisons are made with the numerical results. Next, the probability density function for the areas of cross sections is computed and compared with the results of numerical simulations.

DOI: 10.1103/PhysRevE.84.041107 PACS number(s): 02.50.Ey, 02.50.Ng

I. INTRODUCTION

Three-dimensional Voronoi tessellations provide a powerful method of subdividing space in random partitions and have been used in a variety of fields, such as computational geometry and numerical computing (see, for instance [1] and the references therein), data analysis and compression [2], geology [3], and molecular biology [4,5]. However, in many experimental conditions it is not possible to directly observe the cells themselves, just their planar or linear sections: thus it is of interest to study the relationships between the geometric properties of three-dimensional structures and their lower-dimensional sections [6].

A basic result has been proved in [7]: the intersection between an arbitrary but fixed plane and a spatial Voronoi tessellation is not necessarily a planar Voronoi tessellation. An analysis of some aspects of the sections of Voronoi diagrams can be found in [6]. However, a far as we know, no analytical formulas have been derived for the distributions of the lengths and areas of the planar sections: this is precisely the aim of this paper.

Following [6], a three-dimensional Voronoi diagram will be denoted by $\mathcal{V}$, and section of dimensionality s will be denoted by $\mathcal{V}(s,3)$.

In the next section, some probability density functions used to fit empirical, or simulated, distributions of Voronoi cells size will be reviewed and, in Sec. III, results will be presented on the distribution of the lengths and areas of $\mathcal{V}(2,3)$.

II. PROBABILITY DENSITY FUNCTIONS OF VORONOI TESSELLATIONS

A Voronoi tessellation is said to be a Poisson Voronoi diagram (PVD), denoted by $\mathcal{V}_p$, if the centers generating the cells are uniformly distributed. In the case of one-dimensional PVD, with average linear density λ, a rigorous result can be derived, namely that the distribution of the lengths of the segments has the probability density function

$$p(l) = 4\lambda^2 l \, \exp(-2\lambda l), \tag{1}$$

or, by using the standardized variable $x = l/\langle l\rangle = \lambda l$ [8],

$$p(x) = 4x \, \exp(-2x). \tag{2}$$

No analytical results are known for the distribution of the sizes of Voronoi diagrams in two dimensions (2D) or 3D; typically distributions of the surfaces or volumes of the Voronoi cells are fitted with a three-parameter generalized gamma probability density function (PDF) of the standardized variable x [9,10],

$$g(x;a,b,c) = c\frac{b^{a/c}}{\Gamma(a/c)}x^{a-1}\exp(-bx^c). \tag{3}$$

It should be noted that from $g(x;a,b,c)$ other, simpler, probability density functions can be derived that have been also used to model empirical distributions of PVD: for instance, by setting $a = b$ and $c = 1$, the one-parameter distribution proposed in [8] results in

$$h(x;b) = \frac{b^b}{\Gamma(b)}(x)^{b-1}\exp(-bx), \tag{4}$$

with variance

$$\sigma_h^2 = \frac{1}{c}. \tag{5}$$

Similarly, set $a = b = (3d+1)/2$, $c = 1$, where d is the dimensionality of the cells: Eq. (3) then becomes

$$p(x;d) = \left(\frac{3d+1}{2}\right)^{\frac{3d+1}{2}} x^{\frac{3d-1}{2}}\exp[-(3d+1)x/2], \tag{6}$$

with variance

$$\sigma_p^2 = \frac{2}{3d+1}. \tag{7}$$

This PDF has been shown to give a good fit for Poisson Voronoi diagrams [11], even though it has no free parameters: it will be used in the following to model distributions of the volumes of three-dimensional Voronoi tessellations.

*ferraro@ph.unito.it
†http://www.ph.unito.it/~zaninett/index.html; zaninetti@ph.unito.it

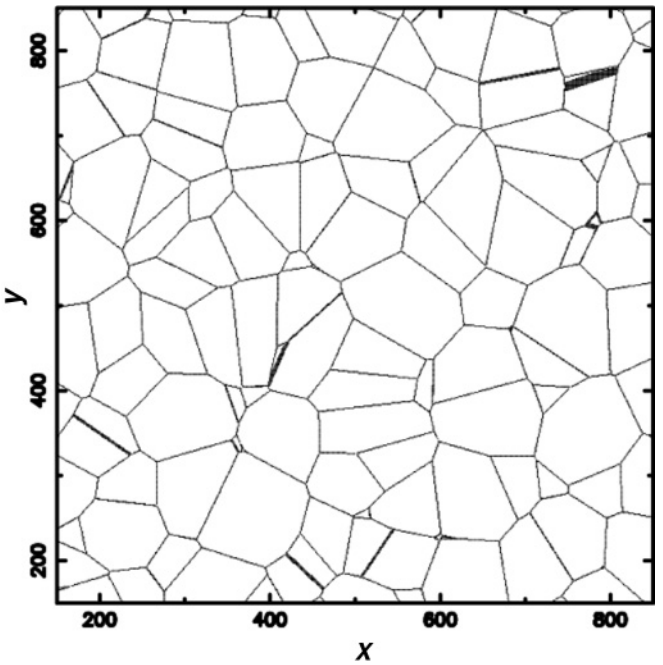

FIG. 1. Planar cross sections of a three-dimensional Voronoi tessellation.

III. SECTIONS

Consider a three-dimensional Poisson Voronoi diagram and suppose it intersects a randomly oriented plane γ: the resulting cross sections are polygons, as in the example shown in Fig. 1.

In order to obtain analytical results for the distributions of the lengths and areas of $\mathcal{V}_p(2,3)$, some simplifying hypothesis is needed: here the cells will be supposed to be spheres. This is, admittedly, a rather rough approximation, but, on the other hand, it makes all cuts of the same simple shape, i.e., circles, irrespective of the orientation of the cutting plane. As shown in the sequel, this approximation allows for deriving an analytical form for the distributions of the radii lengths and the areas of cell sections.

Let $f_V(V)$ be the probability density function for the cell volumes; then the PDF $f_R(R)$ for the lengths of their radii is given by

$$f_R(R) = f_V\left(\tfrac{4}{3}\pi R^3\right)4\pi R^2. \tag{8}$$

The use of Eq. (8) and of the standardized PDF (6), with $d = 3$, leads to

$$f_R(R) = \frac{4\times 10^5}{243}\pi^5 R^{14}\exp\left(-\frac{20}{3}\pi R^3\right). \tag{9}$$

A plot of f_R is shown in Fig. 2.

Consider now the intersection of a sphere of radius R with a randomly oriented plane: the PDF of r, the length of the radius of the resulting circle, is [3]

$$\pi_c(r) = \int_r^\infty f_R(R)\frac{1}{R}\frac{r}{\sqrt{R^2-r^2}}dR. \tag{10}$$

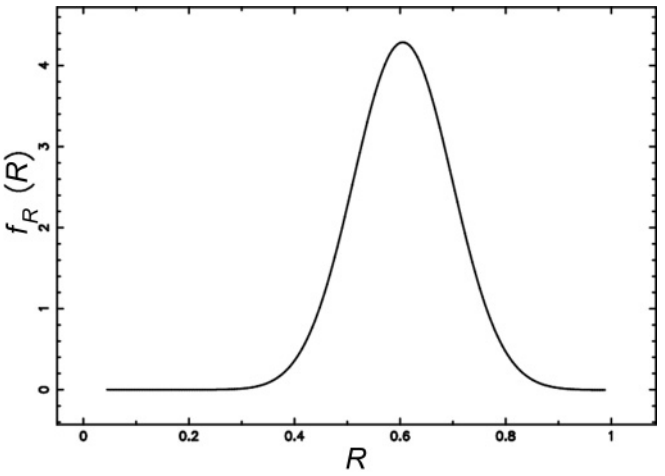

FIG. 2. PDF f_R as a function of R.

The probability of a plane's intersecting a sphere is proportional to R [3] so, in conclusion, the PDF of r can be written as

$$f_r(r) = \alpha\int_r^\infty f_R(R)\frac{r}{\sqrt{R^2-r^2}}dR. \tag{11}$$

Insertion of Eq. (9) into (11) results in the formula

$$f_r(r) = \alpha\frac{4\times 10^5}{243}\pi^5\int_r^\infty R^{14}\exp\left(-\frac{20}{3}\pi R^3\right)\frac{r}{\sqrt{R^2-r^2}}dR. \tag{12}$$

The integral (12) can be solved by making use of a computer algebra system such as MAPLE: the result is

$$f_r(r) = 2/3\alpha\sqrt[6]{3}\sqrt[3]{10}\sqrt[3]{\pi}rG^{4,1}_{3,5}\left(\frac{100}{9}\pi^2 r^6\middle|\begin{matrix}5/6,1/6,1/2\\ 7/3,2/3,1/3,0,\frac{17}{6}\end{matrix}\right), \tag{13}$$

where G is the Mejier G function [12–14]; the numerical value of α, obtained via normalization of f_r, is $\alpha = 1.649$. A plot of f_r is shown in Fig. 3. The Meijer G function is very complicated and Eq. (13) does not lend itself to ready

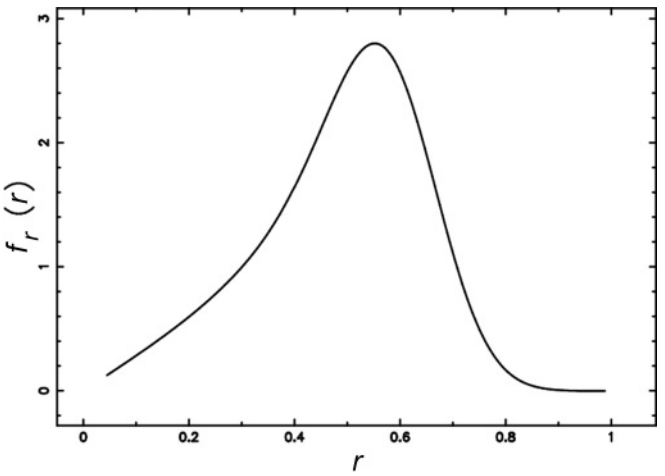

FIG. 3. Probability density function f_r as a function of r.

interpretation; moreover, to the best of our knowledge, it allows no simple approximations (see [15]).

However, some insight into the form of f_r can be gained by considering Taylor expansions. In the interval $[0,0.1]$ f_r is linear, $f_r(r) \approx 2.78r$, while for r close to 1, in the interval $[0.9,1]$, it is well approximated by a quadratic polynomial:

$$f_r(r) \approx -0.006(r-1) + 0.136(r-1)^2. \tag{14}$$

The mode occurs in the interval $[0.5,0.6]$, where a close approximation of f_r is given by

$$f_r(r) \approx 2.48 + 0.58r - 95.528(r-0.55)^2 - 202.18(r-0.55)^3 + 1901.87(r-0.55)^4. \tag{15}$$

From this formula, the mode m can be easily computed: $m = 0.553$.

The mean and variance of f_r are $\langle r \rangle = 0.487$ and $\sigma_r^2 = 0.025$, respectively; f_r is moderately left skewed (skewness $\gamma_r = -0.522$) and is slightly platykurtic (excess kurtosis $k_r = -0.111$). For comparison, note that f_R is more symmetric (skewness $\gamma_R = 0.014$) and has fatter tails (excess kurtosis $k_R = -0.005$).

The distribution function F_r is

$$F_r(r) = \frac{1}{90}\alpha 3^{5/6} 10^{2/3} G^{4,2}_{4,6}\left(\frac{100}{9}\pi^2 r^6 \middle|\begin{matrix}1,7/6,1/2,5/6\\ 8/3,1,2/3,1/3,\frac{19}{6},0\end{matrix}\right)\frac{1}{\sqrt{3}\pi}. \tag{16}$$

The PDF f_A of the areas of $\mathcal{V}_p(2,3)$ can be obtained from f_r by means of the transformation

$$f_A(A) = f_r\left[\left(\frac{A}{\pi}\right)^{1/2}\right]\frac{\pi^{-1/2}}{2}A^{-1/2}, \tag{17}$$

that is,

$$f_A(A) = 0.549\sqrt[6]{3}\sqrt[3]{10}G^{4,1}_{3,5}\left(\frac{100}{9}\frac{A^3}{\pi}\middle|\begin{matrix}5/6,1/6,1/2\\ 7/3,2/3,1/3,0,\frac{17}{6}\end{matrix}\right)\pi^{-2/3}. \tag{18}$$

Since, for r close to 0, $f_r(r) \sim r$ from Eq. (17), it follows that $f_A(0) \neq 0$ and this result has been also verified by numerical simulations we have carried out (see also [6] for a further example). Indeed, it is easy to verify that $f_A(0) = 0.443$. Figure 4 shows the graph of f_A.

The mode of f_A is $m_A = 0.858$, its mean and variance are $\langle A \rangle = 0.824$ and $\sigma_A^2 = 0.204$, respectively; f_A is approximately symmetric (skewness $\gamma_A = 0.278$), and its excess kurtosis is $k_A = -0.337$, indicating that the transformation from f_r to f_A yields a PDF with a lower and broader peak and with shorter and thinner tails.

The distribution function F_A is given by

$$F_A = 0.018\, 3^{5/6} 10^{2/3} G^{4,2}_{4,6}\left(\frac{100}{9}\frac{A^3}{\pi}\middle|\begin{matrix}1,7/6,1/2,5/6\\ 8/3,1,2/3,1/3,\frac{19}{6},0\end{matrix}\right)\frac{1}{\sqrt{3}\pi}. \tag{19}$$

A comparison has been carried out between the distribution functions F_r, F_A, as given by Eqs. (16) and (19), respectively, and the results of a numerical simulation, performed as follows: starting from 300 000 three-dimensional cells, 100 168 irregular polygons were obtained by adding together results of cuts by 41 triples of mutually perpendicular planes.

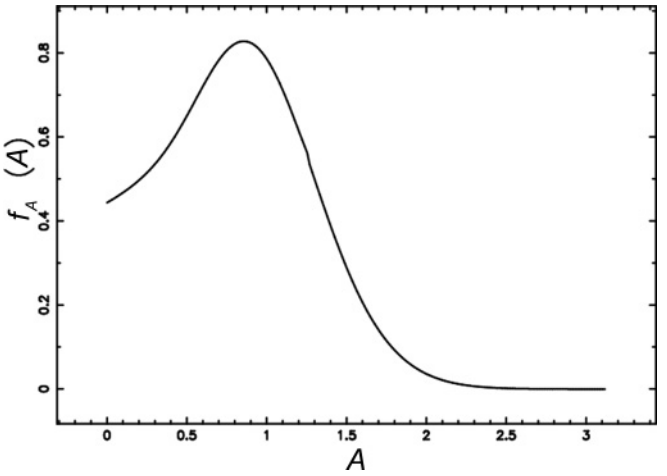

FIG. 4. PDF f_A as a function of A.

The area of the irregular polygons has been obtained with the algorithm described in [16]: briefly, each cut defines a two-dimensional grid and the polygons' areas we measured by counting the number of points of the grid belonging to a given cell.

As concerns the linear dimension, in our approximation the two-dimensional cells were considered circles and thus, for consistency, the radius r of an irregular polygon was defined as

$$r = \left(\frac{A}{\pi}\right)^{1/2}, \tag{20}$$

that is, r is the radius of a circle with the same area of the polygon, A. The empirical distribution of radii is shown in Fig. 5 together with the graph of F_r: the maximum distance between the empirical and analytical curves is $d_{\max} = 0.044$.

Likewise, a comparison between F_A and the simulation is shown in Fig. 6; in this case, $d_{\max} = 0.039$.

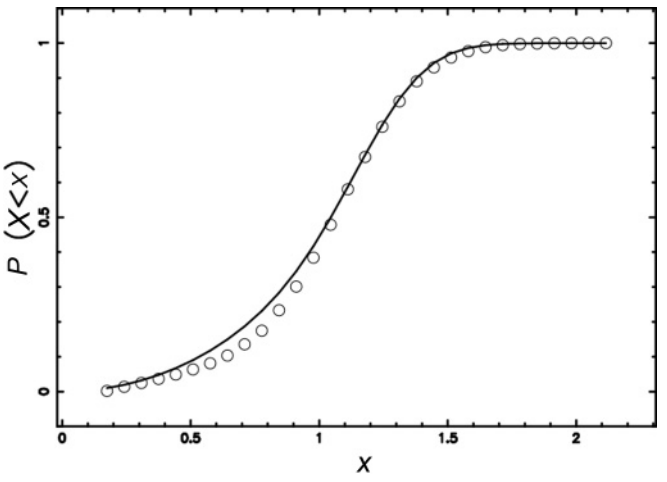

FIG. 5. Comparison between theoretical distribution (continuous line) and data (empty circles) for the distribution of radii r of 2D cells which result from an intersection with a plane. The maximum distance between the two curves is $d_{\max} = 0.044$.

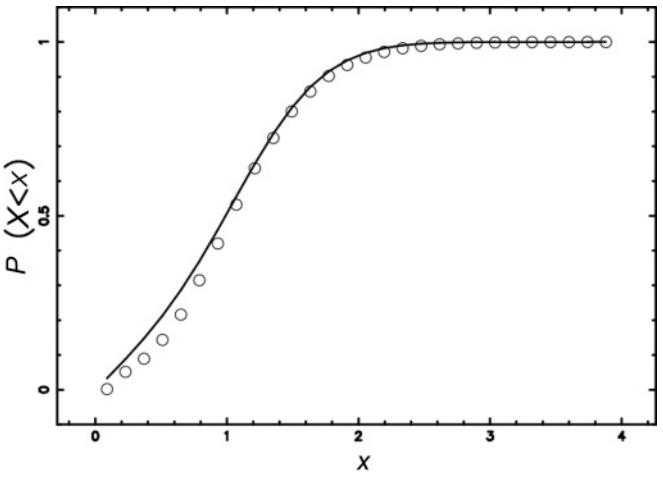

FIG. 6. Comparison between data (empty circles) and theoretical curve (continuous line) of the distribution of areas. The maximum distance between the two curves is $d_{\max} = 0.039$.

IV. CONCLUSIONS

In this paper, analytical formulas have been provided which model the distributions of the lengths and areas of the planar sections of three-dimensional Poisson Voronoi diagrams: in particular, it has been shown that they are related to the Meier G function.

This finding is consistent with the analytical results presented in [17], where it is proved that nonlinear combinations of gamma variables, such as products or quotients, have distributions proportional, or closely related, to the Meijer G distribution.

The analytical distributions F_r and F_A been compared with results of numerical simulations: in evaluating the differences between analytical and empirical distributions, it must be kept in mind that the cells were approximated as spheres and that the distributions used here have no free parameters that can be adjusted to optimize the fit. The results obtained here may be useful for applications in stereology in that they allow for predicting the distributions of linear and planar measures of sections, given an arrangement of three-dimensional cells. This method can also have application to astrophysics, namely in the analysis of the spatial distributions of the voids between galaxies, that are experimentally measured as two-dimensional slices [18] and that can be identified with two-dimensional cuts of a three-dimensional structure. For instance, the distribution of the radius between galaxies of the Sloan Digital Sky Survey Data Release 7 (SDSS DR7) has been reported in [18]; this catalog contains 1054 radii r_e of voids. To compare these experimental data with the results obtained here, one should know the values of R_e, the radii of voids in three dimensions; however by making use of standardized variables $x = r/\langle r\rangle$, $x_e = r_e/\langle r_e\rangle$, one obtains for the standard deviation, based on observations $\sigma_{x_e} = 0.26$, close to the theoretical value, $\sigma_x = 0.32$. Finally, the 2D cuts presented in this paper may be related to Laguerre decompositions (weighted Voronoi decomposition) [19–21], with a weighting factor depending on the distance between the cells and the cutting plane.

[1] Q. Du and D. Wang, SIAM J. Sci. Comput. **26**, 737 (2005).
[2] T. Kanungo, D. M. Mount, N. S. Netanyahu, C. D. Piatko, R. Silverman, and A. Y. Wu, IEEE Transact. Pattern Anal. Mach. Intell. **24**, 881 (2002).
[3] J. Blower, J. Keating, H. Mader, and J. Phillips, J. Volcanol. Geotherm. Res. **120**, 1 (2002).
[4] A. Poupon, Curr. Opin. Struct. Biol. **14**, 233 (2004).
[5] F. Dupuis, J.-F. Sadoc, R. Jullien, B. Angelov, and J.-P. Mornon, Bioinformatics **21**, 1715 (2011).
[6] A. Okabe, B. Boots, and K. Sugihara, *Spatial tessellations. Concepts and Applications of Voronoi diagrams* (Wiley, Chichester, New York, 1992).
[7] S. N. Chiu, R. V. D. Weygaert, and D. Stoyan, Adv. Appl. Probab. **28**, 356 (1996).
[8] T. Kiang, Z. Astrophys. **64**, 433 (1966).
[9] A. L. Hinde and R. Miles, J. Stat. Comput. Simul. **10**, 205 (1980).
[10] M. Tanemura, Forma **18**, 221 (2003).
[11] J.-S. Ferenc and Z. Néda, Phys. A **385**, 518 (2007).
[12] C. Meijer, Nieuw Arch. Wiskd. **18**, 10 (1936).
[13] C. Meijer, Proc. Akad. Wet. Amsterdam **44**, 1062 (1941).
[14] R. A. Askey and A. Olde Daalhuis, in *NIST Handbook of Mathematical Functions*, edited by F. W. J. Olver, D. W. Lozier, R. F. Boisvert, and C. W. Clark (Cambridge University Press, Cambridge, 2010).
[15] J. L. Luke, *The Special Functions and Their Approximations*, Vols. I, II (Academic Press, New York, 1969).
[16] L. Zaninetti, J. Comput. Phys. **97**, 559 (1991).
[17] M. Springer and W. Thompson, SIAM J. Appl. Math. **18**, 721 (1970).
[18] D. C. Pan, M. S. Vogeley, F. Hoyle, Y.-Y. Choi, and C. Park, e-print arXiv:1103.4156 (2011).
[19] H. Telley, Ph.D. thesis, EPFL no. 780, Lausanne (1989).
[20] H. Telley, T. Liebling, and A. Mocellin, Philos. Mag. B: Phys. Condens. Matter Stat. Mech. Electron. Opt. Magn. Properties **73**, 395 (1996).
[21] X. Xue, F. Righetti, H. Telley, T. Liebling, and A. Mocellin, Philos. Mag. B: Phys. Condens. Matter Stat. Mech. Electron. Opt. Magn. Properties **75**, 567 (1997).